Interplay between nematic and cholesteric interactions in self-consistent field theory

Russell K. W. Spencer, Bae-Yeun Ha, and Nima Saeidi

Phys. Rev. E **105**, 054501 — Published 9 May 2022

DOI: 10.1103/PhysRevE.105.054501

Interplay between nematic and cholesteric interactions in self-consistent field theory

Russell K. W. Spencer*,[1,*] Bae-Yeun Ha,[1,†] and Nima Saeidi[2,‡]

[1]*Department of Physics & Astronomy, University of Waterloo, Waterloo, Ontario N2L 3G1, Canada*
[2]*Department of Surgery, The Center for Engineering in Medicine (CEM), Massachusetts General Hospital and Harvard Medical School, Boston, Massachusetts 02114, USA*

(Dated: March 31, 2022)

Chirality is a design feature of a number of biomolecules (e.g., collagen). In these molecules, cholesteric (chiral-nematic) behavior emerges from a combination of the tendency for the biopolymers to align (nematic interactions) and for the alignment direction to change with position, rotating around an axis normal to the alignment direction. This work presents self-consistent field theory (SCFT) of chiral-nematic polymers, which takes into account polymer flexibility and the orientational degrees of freedom of polymer segments. Using the resulting SCFT, we construct a phase diagram showing regions of stability for isotropic, nematic and cholesteric phases. Furthermore, we find that nematic interactions can stabilize the cholesteric phase, pushing the isotropic-cholesteric phase transition to lower cholesteric interaction strength, until the isotropic-nematic-cholesteric triple point is reached.

I. INTRODUCTION

Many macromolecules of biological and technological interest self-assemble into organized structures. In particular, anisotropic (rod-like) molecules can form liquid-crystal phases, such as nematic, smectic and cholesteric (chiral-nematic) phases, among others [1, 2]. Their molecular ordering often dictates the optical [3–8] and mechanical properties of the structures they form [9–13]. Indeed, the ability of these molecules to form desired structures is crucial for their integrity as structural elements in cells or as photonic materials. This is most obvious for corneal collagen, which combines both features: optical and mechanical [9–13]. Some molecules tend to align and can form nematic structures; rodlike molecules without chirality are good examples [1, 2]. Some molecules have chirality; their mirror reflection has an opposite handedness. These molecules can form cholesteric phases, since adjacent molecules tend to align slightly in a non-parallel (skew) orientation (see Fig. 1). Good examples are the structural proteins collagen [9, 14–22] and chitin [23], and DNA [24].

The focus of this paper is on nematic and cholesteric molecules, as illustrated in Fig. 1. Studying chiral molecules is no simple task. First, each molecule stores large degrees of freedom: conformational and orientational. Beyond some length scale known as the persistence length, they tend to coil up, so as to explore a large conformational space. Second, the simultaneous presence of various distinct interactions poses a serious challenge to our theoretical analysis: bending, nematic, chiral interactions, ...

In the Oseen-Frank (OF) model [2, 25], a system of rodlike molecules is represented by a vector field, $\mathbf{n}(\mathbf{r})$, of unit size (i.e., $\mathbf{n}\cdot\mathbf{n}=1$). A free energy cost is assigned to different types of deformations: splay, twist (chiral), and bending. The degree of these deformations is controlled through the coefficients of the corresponding free energy terms. In OF model, the cholesteric free energy density is given by

$$f_{\mathrm{OF\,chol}} = \frac{1}{2}K_{22}\left(\mathbf{n}\cdot\nabla\times\mathbf{n}+\frac{k_2}{K_{22}}\right)^2. \qquad (1)$$

The parameter K_{22} gives the strength of cholesteric interactions and k_2 controls the pitch. This free energy term is minimized by the following cholesteric configuration $\mathbf{n}(z)=\hat{\mathbf{x}}\cos(kz)+\hat{\mathbf{y}}\sin(kz)$, when $k=k_2/K_{22}$, where $\hat{\mathbf{x}}$ and $\hat{\mathbf{y}}$ are unit vectors in the x- and y-directions [2, 25]. Here, $2\pi/k$ is the pitch, i.e., a height along the z axis, over which the director $\mathbf{n}$ makes a complete turn.

The full OF free energy contains more terms that describe splay, bend, splay-bend, and saddle-splay deformations [1, 2]. For instance, the so-called blue phase, characterized by double twist, is controlled by an energy term describing saddle-splay deformations [2, 26, 27]. However, they are not directly relevant to the cholesteric behavior we focus on, as shown in Fig. 1. This work builds on the OF model in Eq. 1.

Although the OF model has been highly successful in predicting the particular configurations of aligned molecules, it has limitations. One typically seeks for $\mathbf{n}$ that minimizes the free energy in Eq. 1 or a more general form of free energy [1, 2, 26, 27]. As a result, it ignores the orientational degrees of freedom of individual molecules, which leads to imperfect molecular alignment, as well as the flexibility of their backbone. The formation of isotropic phases by these molecules points to the significance of the orientational degrees of freedom stored in them [1, 2]. In contrast, the conventional Maier-Saupe (MS) or Onsager theory of nematic phases replies on the orientational distribution of molecules (see Eq. 5 for MS interactions) [1, 2]. The distribution tells us about the degree of ordering. It is desirable to construct

*Electronic address: r6spence@uwaterloo.ca
†Electronic address: byha@uwaterloo.ca
‡Electronic address: nsaeidi@mgh.harvard.edu

a cholesteric interaction at the level comparable to that of MS or Onsager theory. Furthermore, chain flexibility turns out to be a relevant parameter, since it tends to diminish orientational ordering [28].

In our previous work [29], we introduced self-consistent field theory (SCFT) of chiral molecules, which takes into account the orientational degrees of freedom and chain flexibility of these molecules. Here, we extend this approach by including explicitly MS nematic interactions [1, 2, 30]. Using the resulting approach, we discuss the chiral-nematic phase behavior and construct a phase diagram showing regions of stability for isotropic, nematic, and cholesteric phases in the ν-γ plane, where ν and γ are nematic and cholesteric interaction parameters, respectively. The isotropic phase occupies the small ν-γ range. The cholesteric phase becomes stabilized as γ increases. Increasing ν does not always induce a transition to the nematic phase. Indeed, we find that MS interactions can stabilize the cholesteric phase by reducing the free energy cost for orientational ordering, as is more obvious for less stiff polymers including collagen. As a result, the isotropic-cholesteric phase transition is shifted to lower cholesteric interaction strength, as long as ν is larger than the value of ν at which the isotropic-nematic transition occurs.

The main advantage of SCFT is its extensibility to the practically relevant case of cholesteric molecules, possibly mixed with crowding molecules (e.g., proteoglycans), near an interface [10–12]. Indeed, the desire to engineer tissue constructs/substitutes (e.g., cornea and tendon) has generated much interest in understanding how confinement or crowding controls the structure of collagen assembly. Self-consistent field theory is well-suited to the study of confined polymer mixtures (see Ref. [28] for confined nematic molecules). Furthermore, it can be extended to capture the aforementioned other types of deformations as outlined in Ref. [29]. Inclusion of these additional complexities will add to the predictive power and relevance of SCFT.

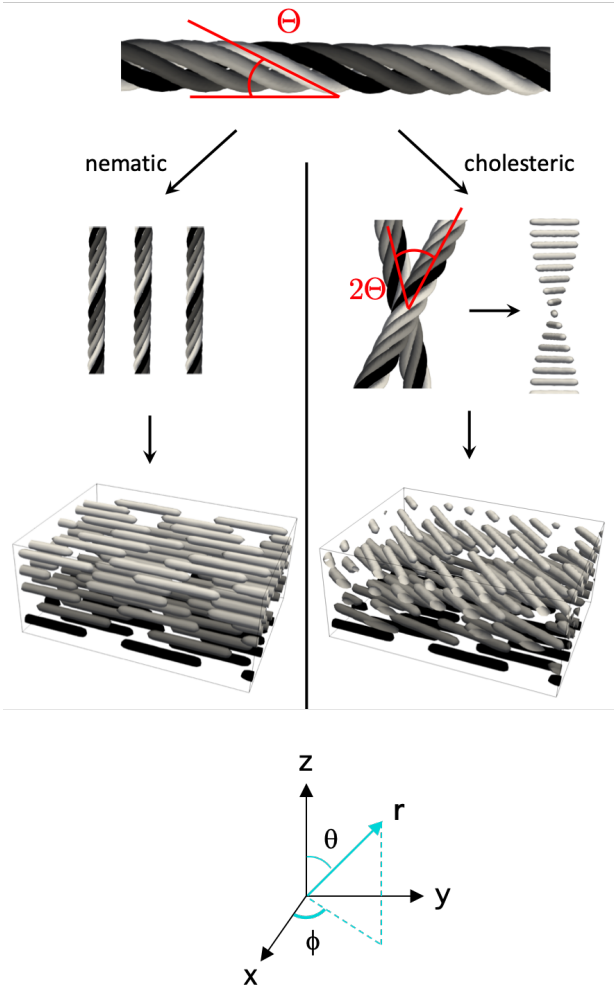

FIG. 1: Molecules that form cholesteric phases tend to be chiral, such as the pentuple helix (resembling type 1 collagen [10–12]) shown at the top. These may align parallel to one another (left) or at an angle (right). If the molecules are thought of as simple solids with the geometry shown, adjacent helices could pack all in parallel (nematic, left) or if successive layers are rotated by an angle 2Θ (with Θ being the twist angle, as defined at the top) then the sub-units of one helix would fit into the grooves between subunits of the adjacent helix. Interactions between real molecules are undoubtedly more complicated, involving weak interactions, such as hydrogen bonding and van der Waals interactions, as well as other complications. This simple picture is only meant to provide an intuitive caricature of the formation of cholesteric phases.

II. THEORY

This work describes an incompressible melt (or solution of uniform concentration) of chiral nematic polymers, modeled as worm-like chains with chiral-nematic interactions. The melt, of volume V, contains n_c chiral polymer chains, each of which has a contour length L and persistence length $\ell_{\rm p}$, as illustrated in Fig. 2. Each polymer is composed of N segments of size a each; each monomer occupies a volume $\rho_0^{-1} = V/n_cN$. The position along the chain is parameterized by s in the range $0 < s < 1$ and the unit tangent vector to a chain is given by

$$\mathbf{u} \equiv \frac{1}{L}\frac{d\mathbf{r}(s)}{ds}, \qquad (2)$$

where $\mathbf{r}(s)$ denotes the spatial position of the segment at location s. The reduced concentration, $\psi(\mathbf{r},\mathbf{u}) \equiv \rho(\mathbf{r},\mathbf{u})/\rho_0$, is the local concentration of segments with orientation $\mathbf{u}$; $\psi(\mathbf{r},\mathbf{u})$ can be thought of as a probability density of segment orientations.

We model interactions between segments using a combination of the Maier-Saupe model [1, 2, 30] and a cholesteric potential that we described in a previous pa-

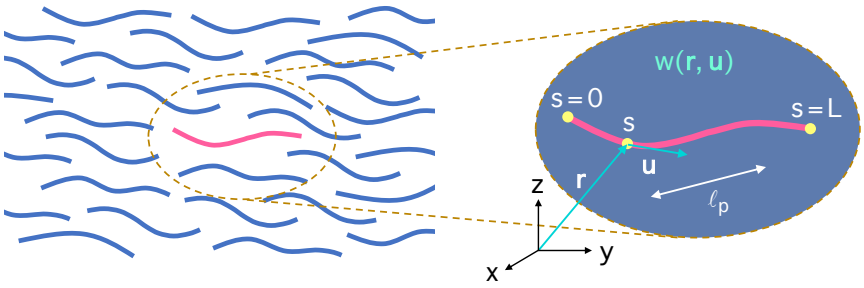

FIG. 2: Collagen-like chains (in a nematic phase) (left) and a field representation (right). The polymers are modeled as worm-like chains with persistent length ℓ_p and contour length L, interacting with each other through chiral-nematic interactions. The field representation focuses on one chain and replaces the influence of others by a field $w(\mathbf{r},\mathbf{u})$ it is subject to. In self-consistent field theory (SCFT), $w(\mathbf{r},\mathbf{u})$ and the spatial distribution of "particles" (e.g., chain segments), denoted as $\psi(\mathbf{r},\mathbf{u})$, are determined self-consistently. We adjust $w(\mathbf{r},\mathbf{u})$ and $\psi(\mathbf{r},\mathbf{u})$ iteratively until they are "correctly" related. "Reprinted with modifications from Ref. [28], R. K. W. Spencer et al, J. Chem. Phys. **152**, 204907 (2020), with the permission of AIP Publishing."

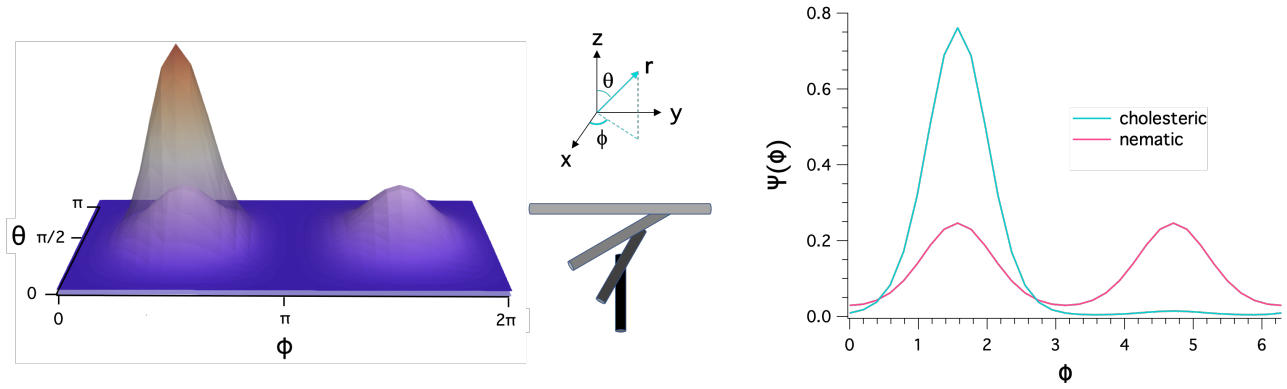

FIG. 3: Distributions, $\psi(\mathbf{r},\mathbf{u})$, are shown for the cholesteric phase (single-peak) and the nematic phase (double-peak), calculated at $\gamma = 4.5133$ and $\nu = 132.528$. The horizontal plot on the left shows the distribution in ϕ-θ space whereas the plot on the right shows a slice through $\theta = \pi/2$. The illustration in the middle is to define the angles ϕ and θ. The rod on top has $\phi = \pi/2$ and $\theta = \pi/2$. This orientation represents the peak location in the ϕ-θ space in the distribution on the left. The distribution is more strongly peaked for the cholesteric phase.

per [29]. The effective Hamiltonian of the melt is given as a sum of several terms:

$$U = U_{\rm B} + U_0 + U_{\rm MS} + U_{\rm C}. \tag{3}$$

Here, $U_{\rm B}$ is a sum of bending energies for the n_c WLCs, each identified by an index α (see Ref. 28 and those therein)

$$\frac{U_{\rm B}}{k_{\rm B}T} = \frac{\ell_{\rm p}}{2L}\sum_{\alpha=1}^{n_c}\int_0^1 ds\left|\frac{d\mathbf{u}_\alpha}{ds}\right|^2. \tag{4}$$

The excluded volume interaction, U_0, is simply a constant for a uniform density and thus can be ignored. The Maier-Saupe interaction is given by [1, 2, 30]

$$\frac{U_{\rm MS}}{k_{\rm B}T} = -\frac{\nu_N\rho_0}{2}\int d\mathbf{r}d\mathbf{u}d\mathbf{u}'\psi(\mathbf{r},\mathbf{u})P_2(\mathbf{u}\cdot\mathbf{u}')\psi(\mathbf{r},\mathbf{u}'), \tag{5}$$

which is characterized by the strength ν and $P_2(x) = (3x^2-1)/2$ is the Legendre polynomial of degree two. Finally, the cholesteric interaction proposed in Ref. 29

$$\frac{U_{\rm C}}{k_{\rm B}T} = \frac{\gamma_N\rho_0}{2}\int d\mathbf{r}d\mathbf{u}\left[\mathbf{u}\cdot\nabla\times\langle\mathbf{u}'\rangle(\mathbf{r}) + \kappa\right]^2\psi(\mathbf{r},\mathbf{u}), \tag{6}$$

depends on the average local alignment vector, $\langle\mathbf{u}'\rangle(\mathbf{r}) \equiv \int d\mathbf{u}'\psi(\mathbf{r},\mathbf{u}')$, the strength of the interaction, γ, and the characteristic cholesteric pitch, $2\pi/k^*$. In Eq. 5 and Eq. 6, ν_N and γ_N are the strength per chain segment and can be expressed as $\nu_N = \nu/N$ and $\gamma_N = \gamma/N$, where ν and γ are the corresponding strength per chain. Below, we use ν and γ.

The free energy (density) in the OF model in Eq. 1 is a special case of Eq. 6. If we assume $\psi(\mathbf{u},\mathbf{r}) = \delta(\mathbf{u}-\mathbf{n}(\mathbf{r}))$ and set $k_2/K_{22} = \kappa$, $U_{\rm C}$ in Eq. 6 per volume reduces to $f_{\rm OF\,chol}$ in Eq. 1. As a result, $2\pi/k^*$ represents correctly the helical pitch only in the limit $\gamma \to \infty$, i.e., when the

entropy of the system is suppressed. Indeed, there is a subtle difference between Eq. (1) and Eq. (6): $|\mathbf{n}| = 1$ in Eq. (1), whereas $|\langle\mathbf{u}\rangle| \leq 1$ in Eq. (6). To see possible consequences of this difference, let us pretend that we lift the constraint $|\mathbf{n}| = 1$ and treat it as representing $\langle\mathbf{u}\rangle$. If we introduce $A \equiv \sqrt{\langle\mathbf{u}\cdot\mathbf{u}\rangle}$, we can express a segment orientation field as $\mathbf{n} = A\,(\hat{\mathbf{x}}\cos kz + \hat{\mathbf{y}}\sin kz)$. This essentially describes the WLC system by only its local average orientation and degree of orientation, A. The energy in Eq. (6) is minimized when $A^2k^* = \kappa$. The combination A^2k in Eq. (6) plays the same role as k in Eq. (1). As a result, the helical pitch is given by the combination $p = 2\pi/k^*A^2L$ [29].

In the next steps, we carry out self-consistent field theory (SCFT) calculations in the usual way [28, 31] (see Fig. 2 for the essence of SCFT). Given a field, $w(\mathbf{r},\mathbf{u})$, which represents the interactions between segments, we can calculate the propagator, $q(\mathbf{r},\mathbf{u},s)$, of a polymer subject to this field. The propagator is the partition function for a portion of a WLC up to a point on the chain, s, which is fixed at spatial position $\mathbf{r}$, and has orientation $\mathbf{u}$. The propagator for a WLC obeys

$$\frac{\partial q}{\partial s} = \left[\frac{L}{2\xi}\nabla_u^2 - L\mathbf{u}\cdot\nabla - w(\mathbf{r},\mathbf{u})\right] q(\mathbf{r},\mathbf{u},s) \qquad (7)$$

which is solved with uniform initial conditions, $q(\mathbf{r},\mathbf{u},s=0) = 1$. The back propagator, $q^\dagger(\mathbf{r},\mathbf{u},s)$, is the partition function for the rest of the chain and is solved similarly, but starting from the other end of the molecule, thus replacing s with $1-s$. Segment concentrations are then given by

$$\psi(\mathbf{r},\mathbf{u}) = \frac{V}{Q}\int_0^1 ds q(\mathbf{r},\mathbf{u},s)q^\dagger(\mathbf{r},\mathbf{u},s) \qquad (8)$$

where

$$Q = \int d\mathbf{r}d\mathbf{u}q(\mathbf{r},\mathbf{u},1) \qquad (9)$$

is the partition function for a WLC subject to the field $w(\mathbf{r},\mathbf{u})$.

What is presented above describes how we find the statistics of polymers subject to the field, $w(\mathbf{r},\mathbf{u})$. We now consider how to calculate $w(\mathbf{r},\mathbf{u})$. The field represents the interactions of a polymer with other polymers and thus reflects the energies described in Eqs. (5) and (6). The field equation found by differentiating the internal energy is given by

$$w(\mathbf{r},\mathbf{u}) = -\int d\mathbf{u}'[\nu P_2(\mathbf{u}\cdot\mathbf{u}')]\psi(\mathbf{r},\mathbf{u}') + \gamma\int d\mathbf{u}'(\mathbf{u}\cdot\nabla\times\langle\mathbf{u}'\rangle + Lk^*)^2\psi(\mathbf{r},\mathbf{u}'), \qquad (10)$$

which represents the potential produced by polymers with a configuration given by $\psi(\mathbf{r},\mathbf{u}')$. The first term corresponds to the Maier-Saupe interactions, while the second corresponds to the cholesteric interactions.

We now have a way of finding the configuration, $\psi(\mathbf{r},\mathbf{u}')$, given the potential, $w(\mathbf{r},\mathbf{u})$, and a way of finding the potential given the configuration. Applying these two conditions simultaneously gives us a self-consistent solution, corresponding to the single most-likely configuration. This is the essence of self-consistent field theory (SCFT). We solve for the self-consistent solution by starting with an initial guess for the field and adjusting it iteratively, using Anderson mixing [32, 33].

SCFT calculations are carried out by starting from an initial guess for $w(\mathbf{r},\mathbf{u})$, followed by calculating the $\psi(\mathbf{r},\mathbf{r})$ as above and adjusting the $w(\mathbf{r},\mathbf{u})$ to satisfy Eq. (10). A mean-square error between the left- and right-hand sides of Eq. (10) of 10^{-4} is sufficient for our calculations. We can then write the free energy per unit chain as

$$\frac{F}{n_c k_B T} = -\ln Q - \frac{1}{2V}\int d\mathbf{r}\mathbf{u}w(\mathbf{r},\mathbf{u})\psi(\mathbf{r},\mathbf{u}). \qquad (11)$$

The equilibrium behavior of chiral nematic polymers was evaluated by imposing a twist angle for the cholesteric phase (and a twist angle of 0 for the isotropic and nematic phases), as described in Ref. 29. The equilibrium cholesteric pitch was calculated by minimizing the free energy with respect to the twist angle, followed by comparing the free energies of the other phases. SCFT calculations were conducted with a spatial resolution of $\Delta = 0.01L$ and an angular resolution of 20 points in the θ direction and 32 points in ψ. Equation (7) is solved with 5×10^4 steps in s, using an Euler step.

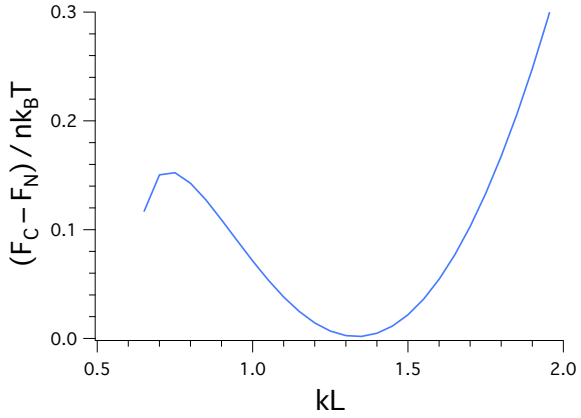

FIG. 4: Free energy, per chain, of the cholesteric phase relative to the isotropic phase, as it varies with k, the magnitude of the helical wave vector. The curve was calculated at $\gamma = 4.5133$ and $\nu = 132.528$.

III. RESULTS

In this work, we consider the behavior of n_c polymer chains contained in a volume V. Each chain consists of

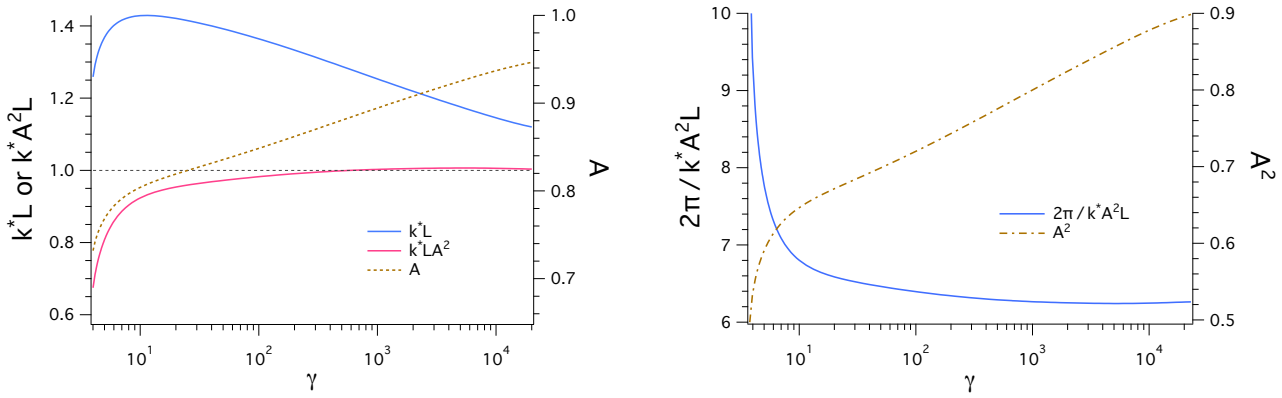

FIG. 5: (Left) Optimal twist wave vector, k^*, and rescaled k^*A^2 (along with the rescaling factor A), obtained with $\nu = 132.528$, as a function of cholesteric interaction strength, γ. The rescaled wave vector k^*A^2 tends to the energy minimizing value of $k^*A^2 = 1/L$ as $\gamma \to \infty$. We did not extend to higher γ as calculations become unstable. (Right) Helical pitch, $p = 2\pi/k^*A^2L$, and A^2 at $\nu = 132.528$ as a function of γ. The helical pitch approaches the expected (energy-minimizing) value 2π, as γ increases.

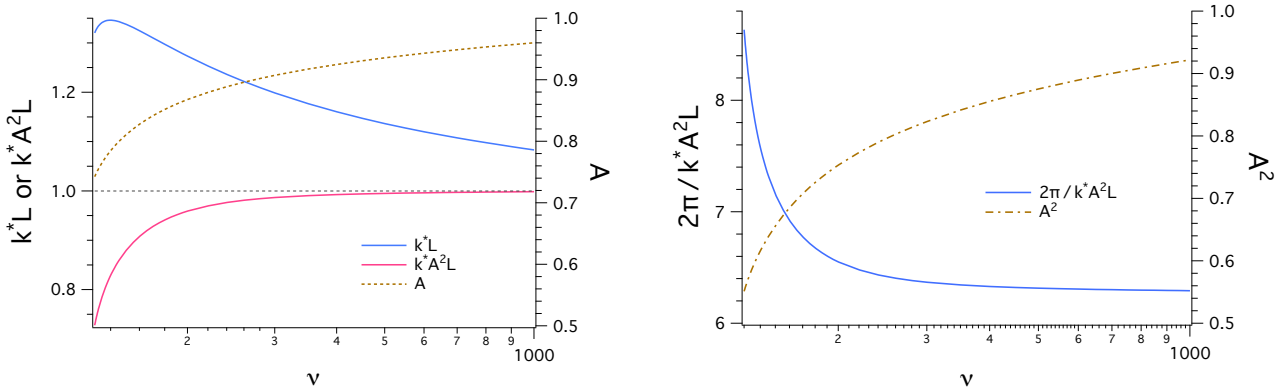

FIG. 6: (Left) Optimal twist wave vector k^*, rescaled wave vector k^*A^2, and A, obtained with $\gamma = 4.5133$, as a function of nematic interaction strength, ν. The rescaled k^*A^2 increases and tends to $1/L$ as ν increases. We did not extend to higher ν as calculations become unstable. (Right) Helical pitch, $p = 2\pi/k^*A^2L$, and A^2 at $\gamma = 4.5133$ as a function of ν. The pitch p approaches 2π, as $\nu \to \infty$.

N monomers and the monomer density is then given by $\rho_0 = n_c N/V$. The chains interact with each other via the Maier-Saupe (MS) and cholesteric (C) interactions described in Eq. 5 and Eq. 6, respectively, in the previous section. Throughout this work, we fix $\kappa = 1$ for simplicity. Changing κ has quantitative but no qualitative effects on the results. Also, we typically use $L/\ell_p = 20$ as for collagen [10, 28, 34], unless otherwise stated.

We start by considering the distributions of orientations of polymers in the phases of interest: cholesteric, nematic, and isotropic. In the isotropic phase, there is no directional preference for monomers or polymers. Thus the distribution is uniform: $\psi(\mathbf{r}, \mathbf{u}) = 1/4\pi$. For the cholesteric and nematic phases, Fig. 3 illustrates typical distributions obtained with $\gamma = 4.5133$ and $\nu = 132.528$. Note that with these parameter choices the isotropic, nematic, and cholesteric phases have the same free energy (see Fig. 8). The monomer orientation distribution in the nematic phase is peaked along $\pm\mathbf{n}$, the nematic director. This reflects the fact that in the nematic phase, a parallel arrangement is equivalent to an anti-parallel arrangement. Polymers may be reversed (reflected) with no change to the relevant physics. Mathematically, we see this as the quadratic dependence of the interaction energy on the dot product $\mathbf{u} \cdot \mathbf{u}'$ in Eq. 5.

In the cholesteric phase, there is a single orientation peak, as shown in Fig. 3. This arises from the nature of cholesteric interactions that depend on the chirality of the molecules. Traveling one direction along the molecules (e.g., increasing s) is different from traveling the other way (decreasing s). Monomers pointing along the $-\mathbf{u}$ direction are reflections of monomers pointing in the $\mathbf{u}$ direction. In chiral molecules, "antiparallel" monomers would therefore have the opposite

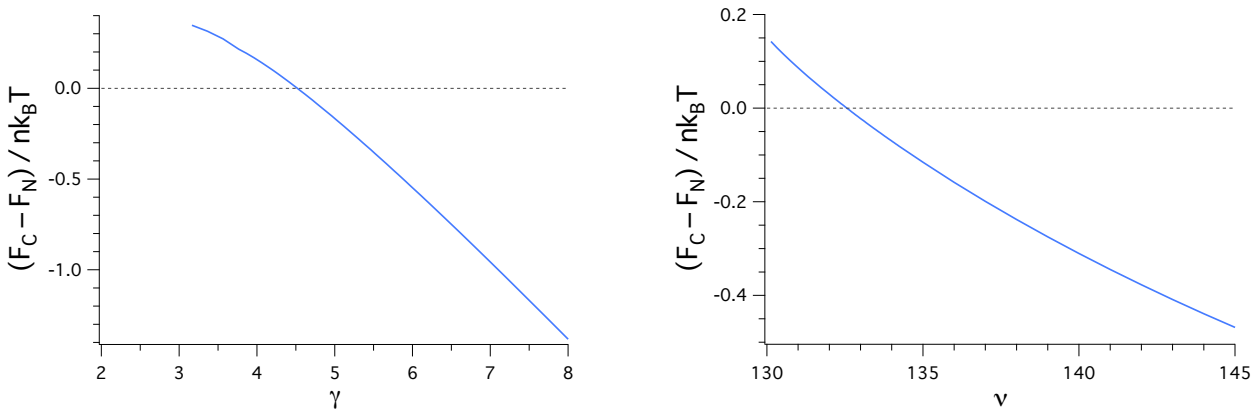

FIG. 7: (Left) Free energy, per chain, of the cholesteric phase relative to the nematic phase, as it varies with cholesteric interaction strength, γ. Free energies are calculated at the optimal twist angle, with the same $\nu = 132.528$ as in Fig. 5. (Right) Free energy, per chain, of the cholesteric phase relative to the nematic phase, as it varies with nematic interaction strength, ν. Free energies are calculated at the optimal twist angle, with the same $\gamma = 4.5133$ as in Fig. 6.

chirality. Mathematically, this enters in the linear term $2k^*\mathbf{u}\cdot\nabla\times\langle\mathbf{u}'\rangle(\mathbf{r})$ in Eq. (6) and leads to a preference for a particular segment orientation and a particular twist direction, i.e., nematic planes rotating clockwise with increasing z in Fig. 1, as opposed to anticlockwise, as would occur for molecules with the opposite chirality.

The next step is to determine the optimal pitch for the cholesteric phase, by evaluating the free energy as a function of k, the magnitude of the helical or twist wave vector. Fig. 4 shows an example calculation obtained with the choices: $\gamma = 4.5133$ and $\nu = 132.528$, as in Fig. 3; in this work, γ is given in units of L^2 but ν is dimensionless. The free energy has a clear minimum, indicating a preference for a particular (optimal) value of k. The cholesteric energy U_C in Eq. 6 is minimized when $k = k^* = 1/L$.

We have three adjustable parameters in this model: the strengths of nematic and cholesteric interactions, denoted as ν and γ respectively, and the preferred pitch of an "ideal" cholesteric phase, $2\pi/\kappa$ (with κ set to 1). We explore the effect of changing the relative strengths of cholesteric and nematic interactions, while fixing $\kappa = 1$.

The graph on the left in Fig. 5 shows how the optimal helical wave vector k^*, obtained with $\nu = 132.528$, changes as we vary the strength of cholesteric interactions γ. As noted earlier and discussed in Ref. 29, the helical pitch is no longer equal to $2\pi/k^*L$ when $|\mathbf{u}| < 1$, as is the case for $\gamma < \infty$. It is larger than $2\pi/k^*L$, since entropy tends to diminish the helical organization, thus stretching the pitch. Also shown is the rescaled k^*L, i.e., k^*A^2L, as well as A (right axis). As γ increases, k^*A^2L increases gradually and approaches 1, at which the cholesteric energy in Eq. 6 is minimized.

The graph on the right in Fig. 5 summarizes our results for the helical pitch $p = 2\pi/k^*A^2L$ along with the calculated values of A^2. The helical pitch decreases monotonically and tends to 2π as γ increases. Only in the limit $\gamma \to \infty$ will the pitch reduce to the one, at which the cholesteric energy in Eq. 6 is minimized: $p = 2\pi$,

We are also interested in k^* as we vary the nematic interaction strength, ν. The graph on the left in Fig. 6 shows k^* as a function of ν for $\gamma = 4.5133$. Once again, at large interaction strength, $k^* \to 1/L$, for the same reason as in Fig. 4: stronger interaction strength leads to a more peaked distribution, $\psi(\mathbf{r},\mathbf{u})$, suppressing entropic effects; for larger ν, the polymers are better aligned and there will be less entropy to lose when forming a cholesteric structure. Also shown in Fig. 6 is k^*A^2 and A, as a function of ν. In contrast to k^*L, k^*A^2L increases gradually and approaches 1, i.e., the energy minimizing value, similarly to what is shown in Fig. 5.

The graph on the right in Fig. 6 shows the helical pitch $p = 2\pi/k^*A^2L$ as a function of ν (along with A^2). The pitch decreases monotonically with ν and approaches the expected limiting value 2π as $\nu \to \infty$. This observation is paralleled by what the right graph in Fig. 5 suggests.

In order to examine the relative stability of the cholesteric and nematic phases, we consider the difference in free energy between these phases as a function of γ. A sample calculation is illustrated in the graph on the left in Fig. 7 obtained with $\nu = 132.528$ as in Fig. 5. At higher cholesteric interaction strengths, the cholesteric becomes more stable. This signals a phase transition to the cholesteric phase.

The relative stability of cholesteric and nematic phases also changes when the nematic interaction strength ν is varied while γ is held fixed at $\gamma = 4.5133$. This is illustrated in the graph on the right in Fig. 7. Strangely, increasing the nematic interaction strength appears to stabilize the cholesteric phase, not the nematic phase. First, note that this is not a general feature of a cholesteric system described by the sum: $U_B + U_{MS} + U_C$ (see Sec. II). For smaller γ (< 4.5133), increasing ν indeed stabilizes the nematic phase, as evidenced below.

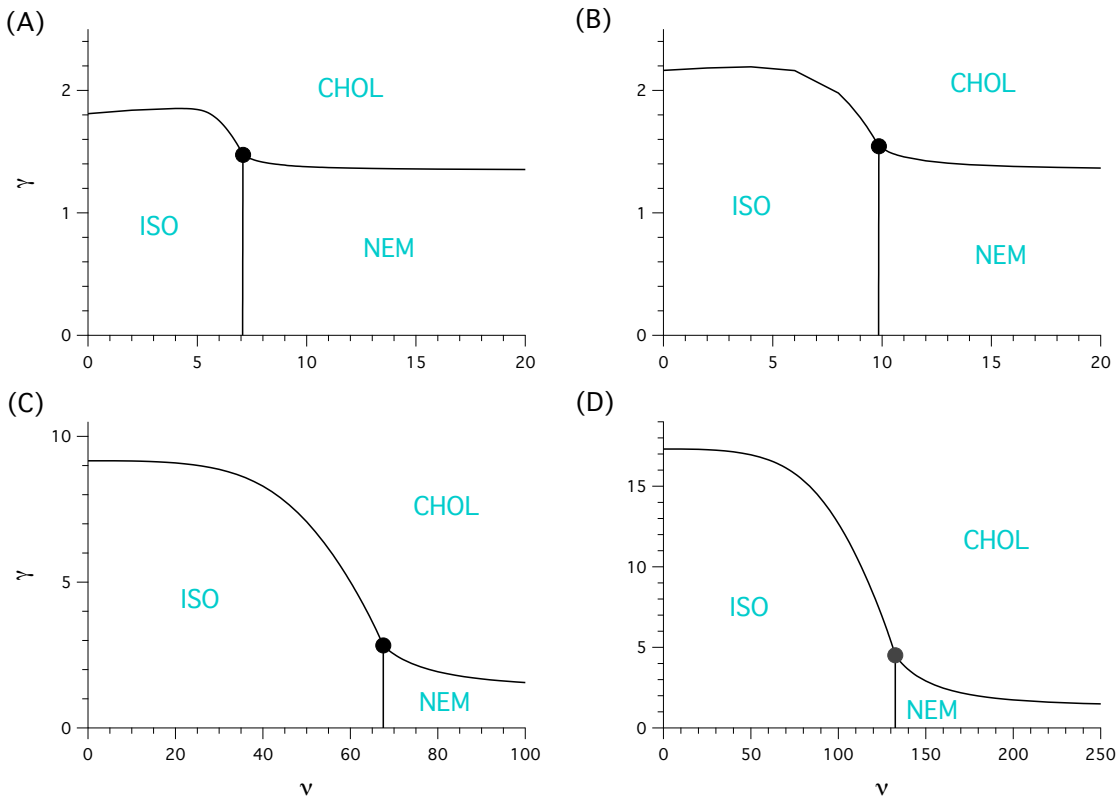

FIG. 8: Phase diagram, depicting the boundaries between the cholesteric, isotropic and nematic phases in the ν-γ space. The diagrams are shown for (A) $L/\ell_{\rm p} = 0.5$ (rod-like), (B) 1, (C) 10, (D) 20 (collagen-like). Here ISO labels the region where the isotropic phase is stable; similarly, CHOL and NEM stand for cholesteric and nematic, respectively. As $L/\ell_{\rm p}$ increases, the polymers become more flexible. As a result, the isotropic phase is stable in a wider space. The dot in each diagram is the triple point, where the three phases coexist.

It proves useful to consider increasing ν for some large γ: $\gamma > 4.5133$. In this case, the cholesterol energy competes with the entropic cost for forming the cholesteric phase. For sufficiently large γ, the competition is tilted toward the cholesteric phase, irrespectively of the nematic energy $U_{\rm MS}$. Otherwise, the system tends to balance $U_{\rm B} + U_{\rm MS} + U_{\rm C}$ with entropy. As ν increases, the entropy becomes less important and the polymers in the system can align better. Whether this will induce a transition to nematic or cholesteric phases depends on the balance between $U_{\rm MS}$ and $U_{\rm C}$. The free energy result in Fig. 6 indicates that once the polymers tend to align, the system can benefit from cholesteric ordering more than from nematic ordering, when $\gamma \gtrsim 4.5133$.

Combining these free energy calculations allows us to construct a phase diagram. Here, the control parameter is $L/\ell_{\rm p}$. The boundary between different phases is where the free energy (per molecule) is the same for the two phases. Recall that free energies are calculated at the optimal twist angle. The boundary is set by the competition between energy and entropy, which is dictated by the value of $L/\ell_{\rm p}$. Fig. 8 shows phase diagrams in the ν-γ space, obtained with different choices of $L/\ell_{\rm p}$: (A) $L/\ell_{\rm p} = 0.5$ (rod-like), (B) 1, (C) 10, (D) 20 (collagen-like). On the diagram, 'ISO,' 'CHOL,' and 'NEM' refer to the isotropic, cholesteric, and nematic phases, respectively. The region labelled as ISO, for instance, is where the isotropic phase is stable; other regions can be understood similarly. Indeed, $L/\ell_{\rm p}$ controls the width of each region (e.g., ISO). The dot is the triple point where all these phases coexist.

The shape and width of the boundaries between different phases are determined by the interplay between entropy, $U_{\rm B}$ (Eq. 4), $U_{\rm MS}$ (Eq. 5), and $U_{\rm C}$ (Eq. 6). Note that the isotropic phase is stable in a wider parameter space for larger $L/\ell_{\rm p}$, i.e., when the polymers are more flexible, since the entropic penalty for forming ordered states is higher, as reflected in the diagram.

First, the boundary between the isotropic and cholesteric phases is convex upward. This means that the cholesteric phase is more easily reached for larger ν, as is most obvious in (D). This is well aligned with the free energy in Fig. 6, which indicates that the cholesteric phase becomes more stable as ν increases, as long as $\gamma \gtrsim 4.5133$ (i.e., above the triple point). For this large range of γ, the cholesteric system can benefit by lowering $U_{\rm C}$ (Eq. 6);

the role of $U_{\rm MS}$ is to align the polymers from an isotopic phase, reducing the entropic penalty for the formation of a cholesteric phase. Indeed, this is best reflected in the diagram in (D), which represents the largest $L/\ell_{\rm p}$ value used in Fig. 8. In this case, the boundary is nearly flat. As a result, increasing ν will promote the formation of a nematic phase, as long as $\gamma \lesssim 4.5133$.

The boundary between the isotropic and nematics phases is straight vertical. For the range of γ below the triple point, the isotropic and nematic transition is controlled by the value of ν, independently of γ, since the cholesteric phase is unstable in this range of γ (see Fig. 5). This explains the shape of this boundary.

In contrast, the boundary between the cholesteric and nematics phase is convex downward. For small γ, increasing ν promotes the formation of nematic phases, as expected. For γ near the triple point, however, increasing ν makes the nematic phase unstable to the cholesteric phase, as is most obvious in (D). This is correlated with the free energy curve in Fig. 6, which indicates that the cholesteric phases is more stabilized for larger ν.

IV. DISCUSSION

We have presented a theoretical approach to a cholesteric system consisting of semiflexible polymers with chirality (e.g., collagen). The resulting approach combines Meier-Saupe (MS) nematic interactions and chiral interactions inspired by the Oseen-Frank (OF) model into self-consistent field theory (SCFT). It thus extends the scope of SCFT to cholesteric molecules. A distinguishing feature of this approach is that the director vector is allowed to vary in orientation and thus follows a probability distribution, which is set by SCFT equations. As a result, it takes into account the entropy of the system, associated with the orientational degrees of freedom. It can benefit from a wide spectrum of theoretical and computational methods developed for SCFT [30, 31]. Indeed, it enables us to study the transition from an isotropic to cholesteric phase, as the strength of cholesteric interactions increases.

Using our approach, we have studied how MS nematic and chiral interactions orchestrate in determining the phase behavior of cholesteric molecules with varying chain stiffness; we have constructed a phase diagram in the ν-γ plane that shows regions of stability for isotropic, nematic, and cholesteric phases. First, the boundaries between different phases merge into a triple point, where all these phases are equally stable. Also, the region, where the isotropic phase stable, is wider for larger $L/\ell_{\rm p}$ (i.e., more flexible). As a result, the coexistence (triple) point of isotropic, nematic, and cholesteric phases shifts towards larger values of ν and γ, as $L/\ell_{\rm p}$ increases.

For collagen-like molecules (i.e., $L/\ell_{\rm p} = 20$), the nematic interactions reduce the entropic penalty for forming ordered structures and can thus stabilize cholesteric phases, unless γ is sufficiently small below the triple point. This is correlated with our observation that MS interactions narrow the distribution of polymer segment orientations (the data not shown). It makes the cholesteric-phase stable region wider than expected from a picture in which chain flexibility is ignored.

Organization of biomolecules into ordered structures often occurs near an interface, presented by the experimental or biological setting, or in the presence of crowding molecules (e.g., proteoglycans) [10–12]. In earlier studies on nematic polymers [28], we showed that planar confinement tends to align the polymers in parallel to the wall; above the onset of nematic transition, this alignment propagates into the bulk phase. Similar considerations with cholesteric molecules will clarify if planar confinement promotes nematic or cholesteric ordering. Another determining factor is the presence of crowding molecules, which controls the assembly of collagen [10–12]. In contrast to what the conventional Oseen-Frank promises, self-consistent-field theory (SCFT) can be extended to take into account this complexity explicitly through energy terms and the associated fields. Also, similarly to the way we formulated the cholesteric energy in Eq. 1 in SCFT, one can include the energy associated with such deformations as splay, splay-bend, and saddle-splay in SCFT as outlined in Ref. [29]. Finally, our SCFT model has an additional parameter, i.e., the density of polymer segments ρ_0, which can be tuned to experimental conditions. Our approach presented here constitutes a first step toward constructing a more complete free energy approach to collesteric molecules in SCFT.

Acknowledgments

This work was funded by the NIH (Grant No. 1R01EY028234-01) and NSERC (Canada). We acknowledge the computational resources of the Shared Hierarchical Academic Research Computing Network (SHARCNET: www.sharcnet.ca) and Compute/Calcul Canada.

[1] M. J. Stephen and J. P. Straley, *Rev. Mod. Phys.*, 1974, **46**, 617–704.
[2] P. G. de Gennes and J. Prost, *The Physics of Liquid Crystals, 2nd edn. Clarendon*, vol. 93 (Oxford University Press, 1993).
[3] J. L. Fergason, *Molecular Crystals*, 1966, **1**, 293–307.
[4] D. K. Yang, J. L. West, L. C. Chien, and J. W. Doane, *J. Appl. Phys.*, 1998, **76**, 1331–1333.
[5] N. Tamaoki, *Adv. Mater.*, 2001, **13**, 1135–1147.
[6] H. Finkelmann, S. T. Kim, A. Muñoz, P. Palffy-Muhoray, and B. Taheri, *Advanced Materials*, 2001, **13**, 1069–1072
[7] V. A. Belyakov, V. E. Dmitrienko, and V. P. Orlov, *So-*

viet Physics Uspekhi, 2007, **22**, 64–88.
[8] D. J. Mulder, A. P. H. J. Schenning, and C. W. M. Bastiaansen, *J. Mater. Chem. C*, 2014, **2**, 6695–6705.
[9] D. F. Holmes, C. J. Gilpin, C. Baldock, U. Ziese, A. J. Koster, and K. E. Kadler, *Proc. Natl. Acad. Sci. U. S. A.*, 2001, **98**, 7307–7312.
[10] N. Saeidi, E. A. Sander, and J. W. Ruberti, *Biomaterials*, 2009, **30**, 6581–6592.
[11] N. Saeidi, E. A. Sander, R. Zareian, and J. W. Ruberti, *Acta Biomater.*, 2011, **7**, 2437–2447.
[12] N. Saeidi, K. P. Karmelek, J. A. Paten, R. Zareian, E. DiMasi and J. W. Ruberti, *Biomaterials*, 2012, **33**, 7366–7374.
[13] *Polymer Liquid Crystals*, ed. A. Ciferri, W. R. Krigbaum and R. B. Meyer, Elsevier, 2012.
[14] Y. Bouligand, *Tissue Cell*, 1972, **4**, 189–217.
[15] M.-M. Giraud-Guille, *Mol. Cryst. Liq. Cryst. Incorporating Nonlinear Optics*, 1987, **153**, 15–30.
[16] M. M. Giraud-Guille, *Calcif. Tissue Int.*, 1988, **42**, 167–180.
[17] M.-M. Giraud-Guille, *J. Mol. Biol.*, 1992, **224**, 861–873.
[18] L. Besseau and M.-M. Giraud-Guille, *J. Mol. Biol.*, 1995, **251**, 197–202.
[19] M. M. Giraud Guille, G. Mosser, C. Helary, and D. Eglin, *Micron*, 2005, **36**, 602–608.
[20] J. E. Kirkwood and G. G. Fuller, *Langmuir*, 2009, **25**, 3200–3206.
[21] A. Deniset-Besseau, G. Mosser, M.-C. Schanne-Klein, and P. De Sa Peixoto, *Optics Express*, 2010, **18**, 1113–1121.
[22] O. F. Aguilar Gutierrez and A. D. Rey, *Langmuir*, 2016, **32**, 11799–11812.
[23] J. F. Revol and R. H. Marchessault, *Int. J. Biol. Macromol.*, 1993, **15**, 329–335.
[24] D. Marenduzzo, E. Orlandini, A. Stasiak, De W. Sumners, L. Tubiana, and C. Micheletti, *Proc. Natl. Acad. Sci.*, 2009, **52**, 22269–22274.
[25] F. C. Frank, *Discuss. Faraday Soc.*, 1958, **25**, 19–28.
[26] A. I. Brown, L. Kreplak, and A. D. Rutenberg, *Soft Matter*, 2014, **10**, 8500-8511.
[27] S. Cameron, L. Kreplak, and A. D. Rutenberg, *Soft Matter*, 2018, **14**, 4772–4783.
[28] R. K. W. Spencer, N. Saeidi, and B.-Y. Ha, *J. Chem. Phys.*, 2020, **152**, 204907.
[29] R. K. W. Spencer, N. Saeidi, and B.-Y. Ha, *J. Chem. Phys.* 2022, **156**, 114902.
[30] G. Fredrickson, *The Equilibrium Theory of Inhomogeneous Polymers* (International Series of Monographs on Physics), Oxford University Press, USA, 2006.
[31] M. W. Matsen, in *Soft Matter, Volume 1: Polymer Melts and Mixtures*, ed. G. Gompper, and M. Schick, Wiley-VCH: Weinheim, 2006, pp. 87–178.
[32] R. B. Thompson, K. O. Rasmussen, and T. Lookman, *J. Chem. Phys.*, 2004, **120**, 31–34.
[33] P. Stasiak and M. W. Matsen, *Euro. Phys. J. E*, 2011, **34**, R21.
[34] M. J. Buehler and S. Y. Wong, *Biophys. J.*, 2007, **93**, 37–43.